Generalized Frequency Division Multiplexing With Flexible Index Modulation Numerology

Ersin Öztürk, Ertugrul Basar, *Senior Member, IEEE*, and Hakan Ali Çırpan, *Member, IEEE*

***Abstract*—In this letter, generalized frequency division multiplexing (GFDM) is combined with index modulation (IM) exploiting the block-based structure of GFDM in an innovative way. The proposed GFDM-IM scheme uses flexible IM numerology to reduce out-of-band (OOB) emission and provides a novel multilayer system model to further benefit from the enhanced distance spectrum of IM. The proposed scheme adapts maximum likelihood successive interference cancellation based near-optimum detector to improve the error performance and reduce the computational complexity. It has been shown that the proposed GFDM-IM scheme achieves better error performance than classical and IM-based orthogonal frequency division multiplexing and GFDM schemes at the same spectral efficiency, and provides an interesting tradeoff among OOB emission, spectral efficiency, and latency.**

***Index Terms*—Fifth generation (5G) wireless networks, generalized frequency division multiplexing (GFDM), index modulation (IM), multicarrier modulation, physical (PHY) layer design.**

I. Introduction

OWING to increasing demand for fully mobile and connected wireless networks, the wireless community continues to investigate advanced radio access technologies toward fifth generation (5G) wireless networks. In this sense, generalized frequency division multiplexing (GFDM) [1] and index modulation (IM) [2] are two physical (PHY) layer schemes that come into prominence due to their appealing advantages over classical schemes. Taking account its strong potential to fulfill the diverse requirements of future wireless networks, the combination of the IM technique with GFDM has been investigated in [3]–[5], where a fixed IM numerology has been considered. In this letter, a novel GFDM-IM scheme, which uses flexible IM numerology along with the near-optimum detector, is proposed to improve out-of-band (OOB) emission, error performance, and computational complexity of the GFDM scheme. The main contribution of this letter is providing a mechanism to optimize OOB emission, spectral efficiency, and latency by applying sparse IM numerology to the edge GFDM subsymbols. As far as we know, this application would be the first attempt to exploit variable-sized IM subblocks with variable number of active subcarriers for GFDM. Besides, in order to enhance the error performance and reduce the computational complexity of the scheme, a new detector, which adapts a maximum likelihood (ML) successive interference cancellation (SIC) based near-optimum detection [5], is developed for the single-input single-output (SISO) GFDM scheme considering the flexible IM numerology, and its theoretical error performance is analyzed. Furthermore, a new system model, which enables multilayer transmission through IM-bits and quadrature amplitude modulation (QAM) bits, is presented. Thanks to this system model, the proposed scheme provides different error performances and spectral efficiencies for QAM and IM bits, and further benefits from enhanced distance spectrum of IM. The block error rate (BLER), OOB emission, and computational complexity of the proposed GFDM-IM scheme are evaluated via computer simulations. It has been shown that the proposed near-optimum, flexible, multilayer GFDM-IM scheme is a strong alternative for future wireless networks due to its improved BLER and computational complexity performance.

Manuscript received May 29, 2018; revised July 10, 2018; accepted August 4, 2018. Date of publication August 9, 2018; date of current version August 23, 2018. The work of E. Basar was supported by the Turkish Academy of Sciences (TUBA) GEBIP Programme. The associate editor coordinating the review of this manuscript and approving it for publication was Prof. Francesco Verde. *(Corresponding author: Ersin Öztürk.)*

E. Öztürk is with the Faculty of Electrical and Electronics Engineering, Istanbul Technical University, Istanbul 34469, Turkey, and also with the Department of Research and Development, NETAŞ, Istanbul 34912, Turkey (e-mail: ersinozturk@itu.edu.tr).

E. Basar is with the Communications Research and Innovation Laboratory (CORELAB), Department of Electrical and Electronics Engineering, Koç University, Istanbul 34450, Turkey (e-mail: ebasar@ku.edu.tr).

H. A. Çırpan is with the Faculty of Electrical and Electronics Engineering, Istanbul Technical University, Istanbul 34469, Turkey (e-mail: cirpanh@itu.edu.tr).

Digital Object Identifier 10.1109/LSP.2018.2864601

II. System Model of GFDM-IM

For a GFDM symbol with M subsymbols, each containing K subcarriers, the mth subsymbol is divided into L_m IM subblocks, each consists of $u_m = K/L_m$ subcarriers. In an IM subblock, only v_m out of u_m available subcarriers are used to transmit QAM symbols and the active subcarrier positions are used to convey additional bits. Thus, each IM subblock can transmit a message of $\alpha_m = v_m \log_2(Q)$ bits carried by the QAM symbols and $\beta_m = \lfloor \log_2 (C(u_m, v_m)) \rfloor$ bits corresponding to active subcarrier indices, where $\lfloor \cdot \rfloor$ denotes the floor function and $C(\mu, \nu)$ is the binomial coefficient. Therefore, QAM-bits and IM-bits that can be mapped to one GFDM-IM subsymbol become $p_m = L_m \alpha_m$ and $g_m = L_m \beta_m$, respectively, and the total number of bits that can be transmitted within the GFDM-IM scheme is given by $P + G$ bits, where $P = \sum_{m=0}^{M-1} p_m$ and $G = \sum_{m=0}^{M-1} g_m$.

According to Fig. 1(a), P information bits enter the transmitter to be carried by the QAM symbols. First, these P bits are split into M groups with p_m bits and then each group of p_m-bits is divided into L_m groups each containing α_m bits. After that, α_m-bit sequences are mapped by Q-ary mappers to create the modulated symbols vector $\mathbf{s}_m^l = \left[s_m^l(1), s_m^l(2), \ldots, s_m^l(v_m)\right]^T$, where $s_m^l(\gamma) \in \mathcal{S}$, for $l = 1, 2, \ldots, L_m$ and $\mathcal{S}$ denotes the

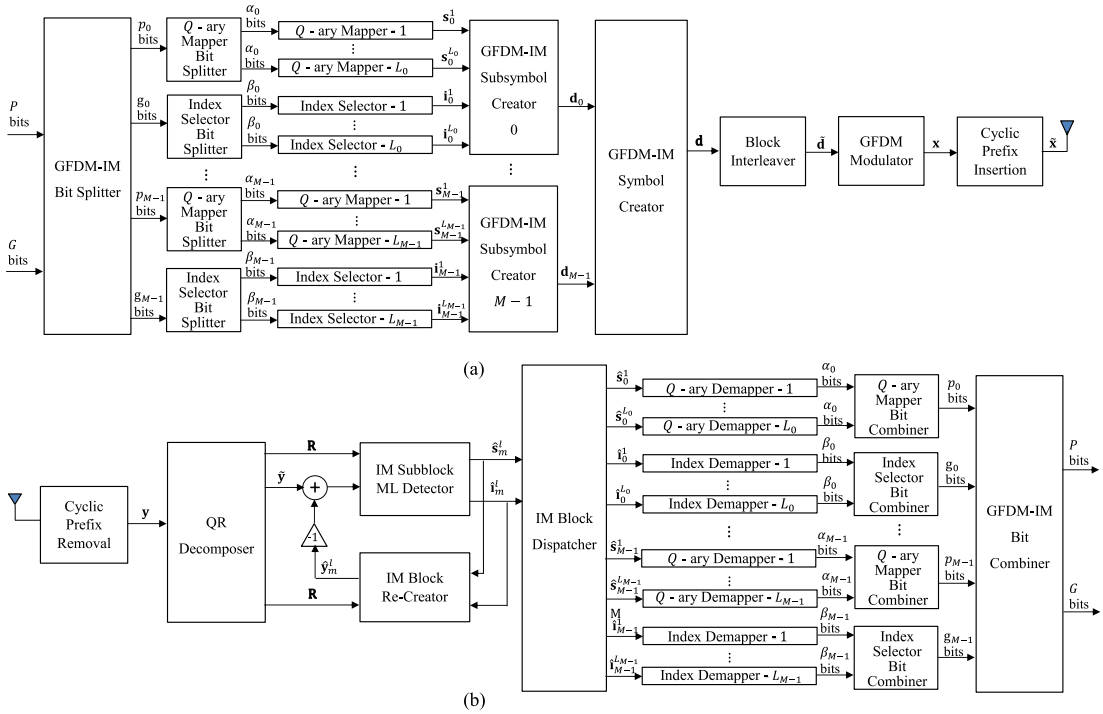

Fig. 1. Block diagram of GFDM-IM. (a) GFDM-IM transmitter. (b) GFDM-IM receiver.

Q-ary signal constellation with Q elements. Meanwhile, G information bits enter the transmitter to be carried by the active subcarrier indices. These G bits are split into M groups with g_m bits first and then each group of g_m-bits is divided into L_m groups each containing β_m bits. These β_m-bit sequences are used by index selectors to select the active subcarrier indices $\mathbf{i}_m^l = \left[i_m^l(1), i_m^l(2), \ldots, i_m^l(v_m)\right]^T$, where $i_m^l(\gamma) \in \{1, \ldots, u_m\}$, by a selection rule. Therefore, $\mathbf{i}_m^l$ has $c_m = 2^{\beta_m}$ possible realizations. Note that the proposed GFDM IM scheme provides two transmission paths with IM and QAM. After that, $\mathbf{s}_m^l$ and $\mathbf{i}_m^l$ vectors are combined to create the GFDM-IM subblocks $\mathbf{d}_m^l = \left[d_m^l(1), d_m^l(2), \ldots, d_m^l(u_m)\right]^T$, where $d_m^l(\gamma) \in \{0, \mathcal{S}\}$, and the resulting GFDM-IM subblocks are concatenated to obtain the GFDM-IM subsymbol $\mathbf{d}_m = [d_{0,m}, d_{1,m}, \ldots, d_{K-1,m}]$. Then, GFDM-IM symbol creator combines the GFDM-IM subsymbols and forms the GFDM-IM symbol

$$\mathbf{d} = [d_{0,0}, \ldots, d_{K-1,0}, d_{0,1}, \ldots, d_{K-1,1}, \ldots, d_{K-1,M-1}] \quad (1)$$

where $d_{k,m} \in \{0, \mathcal{S}\}$, for $k = 0, \ldots, K-1, m = 0, \ldots, M-1$, is the data symbol of kth subcarrier on mth subsymbol. At this point, in order to have uncorrelated channels, a block interleaver with size $L_m \times u_m$ is employed for inner subsymbols of $\mathbf{d}$ and the interleaved data vector $\tilde{\mathbf{d}}$, where $\tilde{d}_{k,m} = d_{(\mathrm{mod}(k,u_m)L_m + \lfloor k/u_m \rfloor), m}$, for $k = 0, \ldots, K-1, m = 1, \ldots, M-2$, is obtained. Here, $\mathrm{mod}(\mu, \nu)$ is the modulo of μ with respect to ν. Then, the resulting GFDM-IM symbol $\tilde{\mathbf{d}}$ is modulated using a GFDM modulator and the GFDM transmit signal becomes $\mathbf{x} = \mathbf{A}\tilde{\mathbf{d}}$, where $\mathbf{A}$ is an $N \times N$ GFDM modulation matrix [1] and $N = KM$. Finally, a cyclic prefix (CP) with length N_{CP} is appended to $\mathbf{x}$ and the resulting vector $\tilde{\mathbf{x}} = [\mathbf{x}(KM - N_{\mathrm{CP}} + 1 : KM)^T, \mathbf{x}^T]^T$ is sent over a frequency-selective Rayleigh fading channel.

At the receiver side, considering the block diagram in Fig. 1(b) and under the assumption that CP is longer than the channel delay spread (N_{Ch}), the received signal vector $\mathbf{y}$ can be expressed as

$$\mathbf{y} = \mathbf{H}\mathbf{x} + \mathbf{w} = \mathbf{H}\mathbf{A}\tilde{\mathbf{d}} + \mathbf{w} = \tilde{\mathbf{H}}\tilde{\mathbf{d}} + \mathbf{w} \quad (2)$$

after the removal of CP. Here, $\mathbf{y} = [y(0), y(1), \ldots, y(N-1)]^T$ is the vector of received signals, $\mathbf{H}$ is the $N \times N$ circular convolution matrix constructed from the channel impulse response coefficients given by $\mathbf{h} = [h(1), h(2), \ldots, h(N_{\mathrm{Ch}})]^{\mathrm{T}}$, and $\mathbf{w}$ is an $N \times 1$ vector of additive white Gaussian noise samples. The elements of $\mathbf{h}$ and $\mathbf{w}$ follow $\mathcal{CN}(0,1)$ and $\mathcal{CN}(0, \sigma_w^2)$ distributions, respectively, where σ_w^2 is the variance of the noise samples.

III. Near-ML Detection of GFDM-IM Scheme

At this stage, in order to realize joint detection and demodulation with reduced complexity, ML-SIC method [5] is developed for SISO GFDM-IM system considering variable-sized IM subblocks. The QR-decomposition [6] of $\tilde{\mathbf{H}}$ is given as $\tilde{\mathbf{H}}\mathbf{\Pi} = \mathbf{Q}\mathbf{R}$, where $\mathbf{Q}$ is an $N \times N$ unitary matrix, $\mathbf{R}$ is an $N \times N$ upper triangular matrix, $\mathbf{\Pi}$ permutes the columns of $\tilde{\mathbf{H}}$ prior to decomposition in order to realize deinterleaving. Then, multiplying the received signals with $\mathbf{Q}^{\mathrm{H}}$ yields

$$\tilde{\mathbf{y}} = \mathbf{Q}^{\mathrm{H}}\mathbf{y} = \mathbf{R}\mathbf{d} + \tilde{\mathbf{w}} \quad (3)$$

where $\tilde{\mathbf{w}} = \mathbf{Q}^{\mathrm{H}}\mathbf{w}$. After that, the ML solution of the last IM subblock is obtained using the upper triangular form of $\mathbf{R}$ and the interference caused by this subblock is removed. Then, the system size is decreased by u_m and the operation continues until the first IM subblock is detected. Algorithm 1 shows the proposed detection method. Here, the subscripts u_m, $\bar{u}_m$, and : denote the last u_m, all but the last u_m, and all elements of the subscripted object, respectively. Finally, the original information bits are obtained by the subsequent blocks.

Algorithm 1: ML-SIC Detection.

1: **Input** $= \tilde{\mathbf{y}}, \mathbf{R}$
2: **Output** $= \hat{\mathbf{s}}_m^l, \hat{\mathbf{i}}_m^l$, for $m = 0, \ldots, M-1, l = 1, \ldots, L_m$
3: **for** $m \leftarrow M-1$ to 0 **do**
4: **for** $l \leftarrow L_m$ to 1 **do**
5: $\hat{\mathbf{d}}_m^l = \underset{\mathbf{I},\mathcal{S}}{\operatorname{argmin}} \| \tilde{\mathbf{y}}_{u_m} - \mathbf{R}_{u_m,u_m} \mathbf{d}_m^l \|^2$
6: $\hat{\mathbf{y}}_m^l = \mathbf{R}_{:,u_m} \hat{\mathbf{d}}_m^l, \tilde{\mathbf{y}} \leftarrow \tilde{\mathbf{y}} - \hat{\mathbf{y}}_m^l$
7: $\tilde{\mathbf{y}} \leftarrow \tilde{\mathbf{y}}_{\bar{u}_m}, \mathbf{R} \leftarrow \mathbf{R}_{\bar{u}_m,\bar{u}_m}$
8: **end for**
9: **end for**

IV. Performance Analysis of GFDM-IM Scheme

In this section, we analytically evaluate the BLER performance of the GFDM-IM scheme using the near-optimum detector. When the channel state information is perfectly known at the receiver, the IM subblock ML detector computes an estimate of the transmitted IM subblock vector according to metric given in line 5 of Algorithm 1. At this point, we deal with the probability that the IM subblock ML detector detects the IM subblock vector $\mathbf{e}_m^l = [e_m^l(1), e_m^l(2), \ldots e_m^l(u_m)]$ instead of $\mathbf{d}_m^l$. In such cases, pairwise error probability (PEP) is used as a measure of error performance. For a given channel realization, taking account of (3), the conditional PEP (CPEP) at the lth stage of the mth subsymbol of ML-SIC receiver can be calculated as

$$P\left(\mathbf{d}_m^l \rightarrow \mathbf{e}_m^l | \mathbf{R}_m^l\right) = P\left(\| \tilde{\mathbf{y}}_m^l - \mathbf{R}_m^l \mathbf{d}_m^l \|^2 > \| \tilde{\mathbf{y}}_m^l - \mathbf{R}_m^l \mathbf{e}_m^l \|^2\right) \quad (4)$$

where $\tilde{\mathbf{y}}_m^l$, $\mathbf{d}_m^l$, and $\mathbf{e}_m^l$ are $u_m \times 1$ vectors, $\mathbf{R}_m^l$ is an $u_m \times u_m$ upper triangular matrix. After some algebra, CPEP at the lth stage of the mth subsymbol of ML-SIC receiver is obtained as [7]

$$P\left(\mathbf{d}_m^l \rightarrow \mathbf{e}_m^l | \mathbf{R}_m^l\right) = Q\left(\sqrt{\frac{\| \mathbf{R}_m^l (\mathbf{d}_m^l - \mathbf{e}_m^l) \|^2}{2\sigma_w^2}}\right) \quad (5)$$

where $Q(x)$ is the Gaussian Q-function. Here, since the distribution of the entries of $\mathbf{R}_m^l$ are complicated, a semianalytical approach can be used to obtain a tight unconditional PEP (UPEP) approximation. In order to perform averaging over $\mathbf{R}_m^l$, $T = 10^6$ samples of $\mathbf{R}_m^l$ are generated as $\mathbf{R}_m^l(t)$, $t = 1, 2, \ldots, T$, and the UPEP at the lth stage of the mth subsymbol of ML-SIC receiver can be obtained as

$$P\left(\mathbf{d}_m^l \rightarrow \mathbf{e}_m^l\right) \approx \frac{1}{T} \sum_{t=1}^{T} Q\left(\sqrt{\frac{\| \mathbf{R}_m^l (\mathbf{d}_m^l - \mathbf{e}_m^l) \|^2}{2\sigma_w^2}}\right) \quad (6)$$

for each signal-to-noise ratio (SNR) value. On the other hand, $P\left(\mathbf{d}_m^l \rightarrow \mathbf{e}_m^l\right)$ is also the probability of incorrect decision for the transmitted IM subblock vector $\mathbf{d}_m^l$ assuming no error at previous stages. Therefore, the probability that all the IM subblock vectors are detected correctly can be shown as

$$P_{\mathcal{C}} = \prod_{m=0}^{M-1} \prod_{l=1}^{L_m} \left(1 - P\left(\mathbf{d}_m^l \rightarrow \mathbf{e}_m^l\right)\right). \quad (7)$$

TABLE I
Computational Complexity of Three Different Receivers

Receiver	*Process*	*Complexity (CMs)*
MMSE	Forming $\widetilde{\mathbf{H}}$, JDD	$N_{\text{Ch}}N^2 + 3N^3 + N^2$
	IM Demod.	$\sum_{m=0}^{M-1} L_m \nu_m c_m Q^{\nu_m}$
	Total	$\sim O\left(3N^3\right)$
ML-SIC	Forming $\widetilde{\mathbf{H}}$, QRD	$N_{\text{Ch}}N^2 + 2N^3 + N^2$
	ML Detection.	$\sum_{m=0}^{M-1} L_m c_m Q^{\nu_m} (u_m \nu_m + u_m)$
	SIC	$N \sum_{m=0}^{M-1} L_m \nu_m$
	Total	$\sim O\left(2N^3\right)$
ML	Forming $\widetilde{\mathbf{H}}$	$N_{\text{Ch}}N^2$
	ML Detection.	$\left(N \sum_{m=0}^{M-1} L_m \nu_m\right) \prod_{m=0}^{M-1} (c_m Q^{\nu_m})^{L_m}$
	Total	$\sim O\left(\left(N \sum_{m=0}^{M-1} L_m \nu_m\right) \prod_{m=0}^{M-1} (c_m Q^{\nu_m})^{L_m}\right)$

As a result, the probability of having at least one error in the detected GFDM block can be expressed as

$$P_{\mathcal{E}} = 1 - P_{\mathcal{C}} = 1 - \prod_{m=0}^{M-1} \prod_{l=1}^{L_m} \left(1 - P\left(\mathbf{d}_m^l \rightarrow \mathbf{e}_m^l\right)\right). \quad (8)$$

Equation (8) is referred as BLER and can be upper bounded by [8]

$$P_{\mathcal{E}} \leq \sum_{m=0}^{M-1} \sum_{l=1}^{L_m} P\left(\mathbf{d}_m^l \rightarrow \mathbf{e}_m^l\right). \quad (9)$$

V. Complexity and OOB Emission Analysis

Computational complexities of classical minimum mean-squared error (MMSE) based joint detection and demodulation (JDD) [3], ML-SIC and ML detectors are analyzed with respect to the number of complex multiplications (CMs) and presented in Table I. From Table I, it is observed that the detector with the proposed ML-SIC technique has the lowest complexity. On the other hand, in [9], an algorithm that exploits the block circularity of $\widetilde{\mathbf{H}}$ has been proposed to reduce the complexity of the classical MMSE detector from cubic to squared order. The application of the algorithm in [9] for GFDM-IM scheme and further enhancements to ML-SIC technique is left for future work.

In GFDM, each subcarrier is filtered individually using a prototype filter. While filtering results nonorthogonality and intercarrier interference, it reduces OOB emission. Since abrupt signal changes between subsequent GFDM blocks cause high OOB emission, in [10], a guard GFDM subsymbol insertion into each block is proposed to achieve more smooth transitions. In this case, OOB emission can be reduced further with a reduced spectral efficiency of $(M-1)/M$. Decrease in the spectral efficiency can be compensated by increasing subsymbol count, which leads to increased latency. As we will show in Section VI, by applying sparse IM numerology to the edge GFDM subsymbols, transitions between GFDM blocks can be smoothed without using guard subsymbol. From Fig. 2, it is observed that using sparse IM numerology at the edge, GFDM subsymbols can reduce OOB emission with a moderate loss in spectral efficiency, hence preventing an increased latency.

VI. Numerical Results

In this section, theoretical and Monte Carlo simulation results for the proposed GFDM-IM scheme are presented for Rayleigh

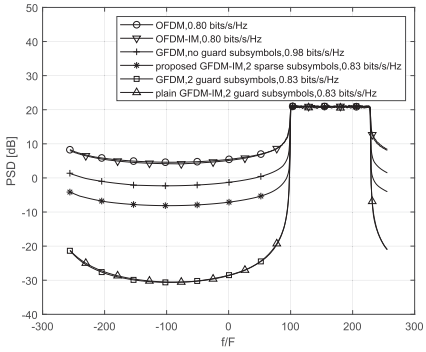

Fig. 2. OOB emission for BPSK transmission.

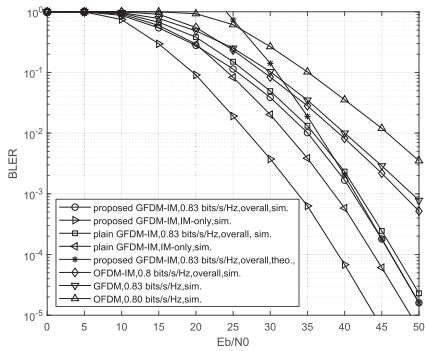

Fig. 3. Uncoded BLER performance for BPSK transmission.

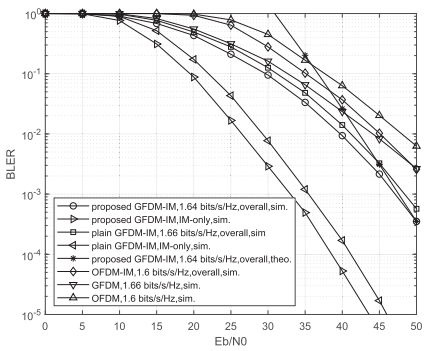

Fig. 4. Uncoded BLER performance for 4-QAM transmission.

TABLE II
LOOKUP TABLE EXAMPLE FOR $u_m = 4$

Bits	*Indices for* $v_m = 2$	*Indices for* $v_m = 3$
[0 0]	{1, 2}	{1, 2, 3}
[0 1]	{2, 3}	{1, 2, 4}
[1 0]	{3, 4}	{1, 3, 4}
[1 1]	{1, 4}	{2, 3, 4}

multipath fading channels with extended pedestrian A channel model. Raised cosine filter with a roll-off factor (a) of 0.1 is used as a GFDM prototype filter. In order to obtain same spectral efficiency, the following system parameters are considered: GFDM and plain GFDM-IM [3] schemes have $M = 13$ subsymbols and their first and last subsymbols are deactivated. The proposed GFDM-IM scheme has $M = 11$ subsymbols and its first and last subsymbols have sparse IM numerology with $u_m = 32, v_m = 1$. For inner GFDM subsymbols for both plain GFDM-IM and the proposed GFDM-IM schemes, u_m is chosen as 4, and v_m is chosen as 2 and 3 for binary phase shift keying (BPSK) and 4-QAM transmissions, respectively, and the active subcarrier positions are determined using the lookup table in Table II. A GFDM block includes 1 GFDM symbol and an orthogonal frequency division multiplexing (OFDM) block includes 11 OFDM symbols with $K = 128$, $N_{\text{CP}} = 32$. Plain GFDM-IM scheme uses classical MMSE detector as in [3], and both the proposed GFDM-IM and the GFDM schemes use ML-SIC detector.

Fig. 2 shows the OOB emission of classical and IM-based GFDM and OFDM schemes for BPSK transmission for the given system parameters. From Fig. 2, it is observed that smooth transitions provided by sparse IM numerology yields 6 dB additional OOB emission suppression with respect to GFDM scheme at the expense of reduced spectral efficiency. On the other hand, while the proposed GFDM-IM scheme reduces OOB emission suppression of GFDM and plain GFDM-IM schemes by approximately 20 dB at the same spectral efficiency, it provides 15% shortening of the symbol length and still provides 13-dB OOB emission suppression with respect to OFDM. The OOB emission suppression of the proposed GFDM-IM scheme can be increased with more sparse subcarrier usage at the expense of reduced spectral efficiency or increased latency. Consequently, the proposed flexible IM numerology can provide an attractive tradeoff among OOB emission, spectral efficiency, and latency, and has significant advantages for fragmented spectrum usage.

Fig. 3 compares the uncoded BLER performance of the proposed GFDM-IM scheme with the plain GFDM-IM scheme, OFDM-IM scheme [11], as well as the classical GFDM and OFDM schemes for BPSK transmission. Here, IM-only curves belong to the bits conveyed by the indices of the active subcarriers and the spectral efficiency of the GFDM-IM schemes are given by $(P + G)/(N + N_{\text{CP}})$ [b/s/Hz]. From Fig. 3, for a target BLER value of 10^{-3}, it is observed that the proposed GFDM-IM scheme achieves 0.8 and 5 dB better BLER performance than the plain GFDM-IM scheme [3] considering overall and IM-only performances, respectively, at the same spectral efficiency. Note that the ML-SIC detector provides a significant improvement for IM-only transmission in terms of BLER and this improvement can be exploited to provide different quality of service classes. On the other hand, BLER performance gains of the proposed GFDM-IM scheme with respect to OFDM-IM, GFDM, and OFDM schemes are risen to 6, 8, and 14 dB, respectively. According to Table I, the computational complexity of the ML-SIC and the classical MMSE detectors required to implement the receiver block of the proposed GFDM-IM scheme are on the order of $\sim\mathcal{O}(5.6 \times 10^9)$ and $\sim\mathcal{O}(8.4 \times 10^9)$, respectively. As a result, the ML-SIC technique provides 34% less complexity with respect to the classical MMSE detector. Fig. 4 shows the BLER performance for 4-QAM transmission. From Fig. 4, it is found that the proposed GFDM-IM scheme provides the similar BLER gains as in BPSK transmissions with respect to other methods. The performance improvements provided by the ML-SIC detector with respect to the classical MMSE detector are the result of joint detection and GFDM-IM demodulation. Besides, performance improvement of GFDM-IM with respect to GFDM is the result of coding gain due to enhanced distance spectrum of IM. For comparison, the theoretical upper bounds obtained from (9) are also depicted in Figs. 3 and 4. As shown in Figs. 3 and 4, the theoretical upper bounds become relatively tight with the simulation results as the SNR increases.

VII. CONCLUSION

In this letter, a novel GFDM-IM scheme, which uses flexible IM numerology along with the near-optimum detector, has been proposed. It has been shown that the proposed GFDM-IM scheme achieves better error performance due to joint detection, GFDM, and IM demodulation, and provides an interesting tradeoff among OOB emission, spectral efficiency, and latency. We conclude that the near-optimum, flexible, multilayer GFDM-IM scheme is a convenient PHY scheme for future wireless networks. Our future works will focus on efficient detection techniques and high mobility implementation.

REFERENCES

[1] N. Michailow *et al.*, "Generalized frequency division multiplexing for 5th generation cellular networks," *IEEE Trans. Commun.*, vol. 62, no. 9, pp. 3045–3061, Sep. 2014.

[2] E. Basar, M. Wen, R. Mesleh, M. Di Renzo, Y. Xiao, and H. Haas, "Index modulation techniques for next-generation wireless networks," *IEEE Access*, vol. 5, pp. 16693–16746, 2017.

[3] E. Ozturk, E. Basar, and H. Cirpan, "Generalized frequency division multiplexing with index modulation," in *Proc. IEEE GLOBECOM Workshops*, Washington, DC, USA, Dec. 2016, pp. 1–6.

[4] E. Ozturk, E. Basar, and H. Cirpan, "Generalized frequency division multiplexing with space and frequency index modulations," in *Proc. 5th IEEE Int. Black Sea Conf. Commun. Network*, Istanbul, Turkey, Jun. 2017, pp. 1–5.

[5] E. Ozturk, E. Basar, and H. Cirpan, "Generalized frequency division multiplexing with flexible index modulation," *IEEE Access*, vol. 5, pp. 24727–24746, Oct. 2017.

[6] D. Wubben, R. Bohnke, J. Rinas, V. Kuhn, and K. Kammeyer, "Efficient algorithm for decoding layered space-time codes," *IEE Electron. Lett.*, vol. 37, no. 22, pp. 1348–1350, Oct. 2001.

[7] E. Basar, "On multiple-input multiple-output OFDM with index modulation for next generation wireless networks," *IEEE Trans. Signal Process.*, vol. 64, no. 15, pp. 3868–3878, Aug. 2016.

[8] Z. Yan, K. M. Wong, and Z. Q. Luo, "Optimal diagonal precoder for multiantenna communication systems," *IEEE Trans. Signal Process.*, vol. 53, no. 6, pp. 2089–2100, Jun. 2005.

[9] M. Matthe, D. Zhang, I. Gaspar, and G. Fettweis, "Reduced complexity calculation of LMMSE filter coefficients for GFDM," in *Proc. IEEE 28nd Veh. Technol. Conf.*, 2015, pp. 1–2.

[10] M. Matthe, N. Michailov, I. Gaspar, and G. Fettweis, "Influence of pulse shaping on bit error rate performance and out of band radiation of generalized frequency division multiplexing," in *Proc. IEEE Int. Conf. Commun. Workshops*, 2014, pp. 43–48.

[11] E. Basar, Ü. Aygölü, E. Panayırcı, and H. V. Poor, "Orthogonal frequency division multiplexing with index modulation," *IEEE Trans. Signal Process.*, vol. 61, no. 22, pp. 5536–5549, Nov. 2013.